IEEE Access
Multidisciplinary | Rapid Review | Open Access Journal

Received 3 November 2023, accepted 8 January 2024, date of publication 8 February 2024, date of current version 21 February 2024.

Digital Object Identifier 10.1109/ACCESS.2024.3364115

RESEARCH ARTICLE

ECG Classification With Event-Driven Sampling

MARYAM SAEED[1], (Member, IEEE), OLEV MÄRTENS[2], (Senior Member, IEEE), BENOIT LARRAS[3], (Member, IEEE), ANTOINE FRAPPÉ[3], (Senior Member, IEEE), DEEPU JOHN[1], (Senior Member, IEEE), AND BARRY CARDIFF[1], (Senior Member, IEEE)

[1]UCD School of Electrical and Electronic Engineering, UCD Engineering and Materials Science Centre, Belfield, Dublin 4, Ireland
[2]Thomas Johann Seebeck Department of Electronics, Tallinn University of Technology, 19086 Tallinn, Estonia
[3]Univ. Lille, CNRS, Centrale Lille, Junia, Univ. Polytechnique Hauts-de-France, UMR 8520-IEMN, 59000 Lille, France

Corresponding author: Maryam Saeed (saeedmaryamali@gmail.com)

This work was supported in part by the CHIST-ERA grant JEDAI CHIST-ERA-18-ACAI-003, the French Research Agency project ANR-19-CHR3-0005-01, EU Regional Development Fund (Estonian Centre of Excellence in ICT Research EXCITE TAR16013), Mobilitas+ project Mobera20, Irish Research Council under the New Foundations Scheme and Schlumberger Foundation's Faculty for the Future program.

ABSTRACT Electrocardiogram (ECG) data's high dimensionality challenges real-time arrhythmia classification. Our approach employs functional approximation to condense ECG recordings into a compact feature set for simpler classification using Chebyshev polynomials. These polynomials, with 200 time points and 80 coefficients, accurately represent arrhythmias in an 81×1 feature vector. We prove Chebyshev polynomials act as implicit low-pass filters on input signals. Using MIT-BIH Arrhythmia and MIT-BIH Supraventricular Arrhythmia datasets, we introduce classifiers that achieve significant accuracy. A three-layered Artificial Neural Network yields high F1-scores (0.99, 0.90, 0.93, and 0.76 for classes N, S, V, and F) with minimal parameters (20,964), surpassing existing models. Furthermore, our proposed ECG classification system exhibits minimal computational demands, requiring only 0.1 MIPS per beat. We also propose efficient signal reconstruction methods, with the iterative approach showcasing accurate reconstruction with negligible error. This approach accommodates various data sampling types and determines optimal Chebyshev coefficients for capturing signal bandwidth.

INDEX TERMS Level-crossing ADC, electrocardiograms, functional approximation, Chebyshev polynomials, artificial neural networks, arrhythmia, support vector machines, bandwidth analysis.

I. INTRODUCTION

Arrhythmia, an abnormal heart rhythm, is a significant medical condition. Atrial fibrillation, the most common form of arrhythmia, is projected to affect millions of people in the United States and Europe in the coming decades [1]. Automated arrhythmia classification is a widely researched area that can help with early diagnosis and improve patient care by providing long-term remote cardiac monitoring. Several hardware-friendly designs have been proposed for real-time arrhythmia classification. Notably, the literature includes real-time patient-specific ECG classifiers as demonstrated in prior works such as Malik et al. [2], Tang et al. [3], and Kiranyaz et al. [4]. Abubakar and colleagues [5] introduced a wearable long-term ECG processor for arrhythmia classification, employing a reduced feature set. Additionally, a low-complexity antidictionary-based ECG classifier was proposed by Duforest et al. [6]. Tang et al. [7] presented a patient-specific arrhythmia classifier with low complexity, utilizing support vector machines. Another promising approach for real-time wearable arrhythmia classification involves utilising a novel sampling technique at the analogue front end, employing level-crossing ADCs (LC-ADCs).

Recent research has demonstrated a growing interest in LC-ADCs due to their potential to reduce data streams and battery consumption. Li et al. [8] introduced an ECG front-end featuring an LC-ADC, showcasing its potential for low-power, high-performance applications. In a different

The associate editor coordinating the review of this manuscript and approving it for publication was Zhan-Li Sun.

approach, Marisa et al. [9] presented a pseudo-asynchronous LC-ADC with dynamic comparators for implantable biomedical sensing. This design offers energy efficiency, a smaller chip area, and robust performance in noisy conditions, making it suitable for long-term sensing applications. Ravanshad et al. [10] introduced an asynchronous analogue-to-digital conversion system utilizing a modified LC-ADC for measuring ECG RR intervals. This system achieved high accuracy, sensitivity, and low power consumption, making it viable for wearable wireless ECG sensors in body-sensor networks. Furthermore, Tlili et al. [11] employed an LC-ADC for ECG signal measurement and proposed a biosignal-dependent design methodology to minimise distortion. Their design exhibited excellent signal quality and robustness against non-idealities, making it a promising choice for ECG data acquisition.

More recently, Van and Gielen [12] introduced a new LC-ADC for biomedical signal acquisition, which mitigated common issues like power consumption and signal-dependent distortion. Similarly, Wei et al. [13] introduced an LC-ADC with adaptive sampling. Their design, utilizing a 180-nm CMOS process, achieved outstanding power efficiency consuming just $197nW$, while still delivering 6.4bits of effective resolution and a signal-to-noise and distortion ratio (SNDR) of 41.6dB. Tang et al. [14] introduced a novel second-order level-crossing sampling ADC for real-time data compression and feature extraction in ECG applications. Their system efficiently separated sampling and quantization processes, achieving a compression factor of 8.33 for sparse ECG signals, and proved to be suitable for low-power sensors. Lin et al. [15] reduced energy consumption in biological signal acquisition by using non-uniform sampling and fixed windows. The LC-ADC achieved 9.51-bit ENOB in 0.18μm CMOS technology. Tong et al. [16] introduced an energy-efficient fixed-window LC-ADC for biomedical applications. With a single continuous-time comparator and integrated digital circuitry, it achieved 73.1 dB SNDR and 20.1μW power consumption at 1 kHz in 0.18μm CMOS technology, offering compact design suitability for biomedical applications.

Existing literature demonstrates that LC-ADCs can achieve data compression of up to 3x, and event-driven arrhythmia classifiers demand only 50% of the computational resources compared to standard classifiers designed for uniformly sampled data [17]. The majority of current ECG classifier systems are tailored for uniformly sampled data, whereas LC-ADCs generate non-uniformly sampled data. These existing designs are not readily applicable to the non-uniform data produced by LC-ADCs. Consequently, there is a pressing demand for algorithms capable of harnessing event-driven data from LC-ADCs for automated arrhythmia detection, with a focus on minimizing power consumption. Fig. 1 shows an illustration of uniform sampling using a conventional ADC and event-driven sampling using an LC-ADC. In conventional ADCs, sampling occurs at regular time intervals, producing quantized amplitude values. In contrast,

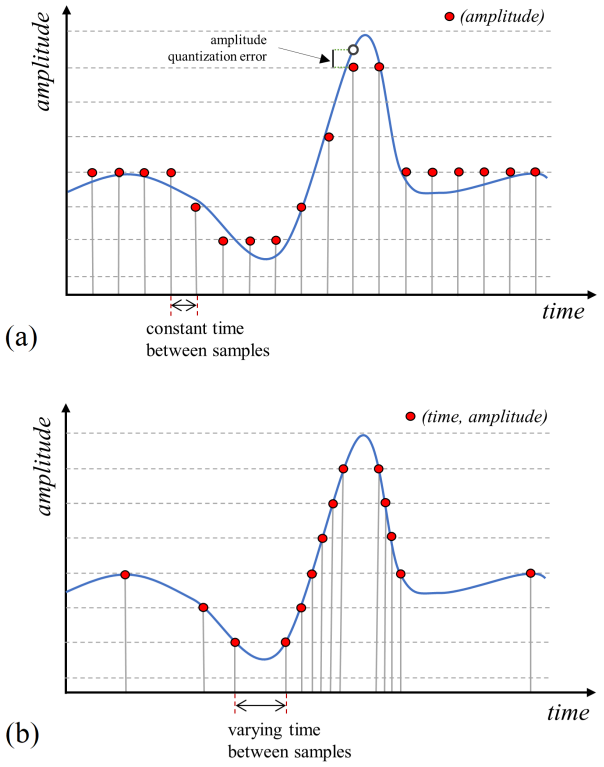

FIGURE 1. (a) uniform sampling using a conventional ADC (b) event-driven sampling using an LC-ADC.

LC-ADCs utilize an event-driven sampling scheme where samples are taken only when the input signal crosses predefined levels - each output is thus a two-dimensional quantity comprising a time and amplitude coordinate. This activity-dependent sampling makes them suitable for sporadic signals, e.g. an ECG signal, resulting in lower average sampling rates and reduced power consumption.

An interesting aspect of LC-ADC is the theoretical absence of amplitude quantization error - when the LC-ADC indicates that a level was crossed, it does so with arbitrary accuracy. Of course, there are other sources of '*noise*' arising from this sampling process as examined by Tili et al. [11], [18], Ravanshad et al. [10] and Saeed et al. [17] - in particular the number of levels used, how accurately they are defined, and the quantization of the time coordination of each sample. Quantization figures of merit are difficult to define as they are very signal-dependent, making the choice of LC-ADC parameters domain-specific. To address this, a recent study [17] used the MIT-BIH Arrhythmia database to develop a good set of parameters, as shown in Table 1, for the application of ECG monitoring. This configuration will be used throughout this paper.

One challenge encountered in event-driven ECG is the varying length of the two-dimensional output, consisting of *"time, amplitude"* pairs. This output cannot be directly utilized by a classifier, leading to difficulties in analysis

TABLE 1. The LC-ADC parameters used for simulation of event-driven ECG datasets.

Parameter	Value
Clock Frequency	2385Hz
Resolution	7-bit
Counter	6-bit
Dynamic Range	10mVpp

and classification. Although non-uniformly sampled data is prevalent in numerous fields such as astronomy, medicine, image processing, communication, and the automotive industry, limited research has been conducted on transforming such data into standard feature sets for classification purposes [19], [20], [21].

A promising approach worth exploring is the spectral analysis of non-uniformly sampled data [22]. Non-uniform fast Fourier transforms (NUFFTs) have gained significant attention as efficient algorithms for computing the discrete Fourier transform (DFT) of non-uniformly sampled data [23], [24]. NUFFTs find applications in various domains, including signal processing, imaging, and computational science [24], [25].

Approximation techniques provide a simplified approach to analyze and interpret complex signals. Functional approximation, in particular, has shown its value in classifying smooth time-series data. By estimating an unknown underlying function based on a given set of observations, a functional approximation can handle irregularly spaced time samples derived from a continuous signal. This method effectively summarizes high-dimensional signals using a standard set of features, eliminating the need for complex deep-learning algorithms to learn features. The work of Melchert et al. [26] emphasizes the effectiveness of using approximation coefficients as features in non-equidistant and non-uniform datasets. Their findings demonstrate the ability of approximation coefficients to compensate for missing data and irregular sampling.

This work builds on the research presented by Saeed et al. [27] with an expansion on the methodology and analysis of the classification of functional approximation features using Chebyshev polynomials. The main novel contributions are: a) functional approximation is used to estimate a feature set from event-driven ECG signals, b) a discrete cosine transform is used for faster coefficient calculation, c) bandwidth analysis of Chebyshev polynomials is presented, d) three new class-oriented classifiers are used to demonstrate the accuracy of classification using functional approximation features, and e) methodologies for accurate reconstruction of ECG signals are compared.

II. METHODOLOGY

A. FUNCTIONAL APPROXIMATION FOR FEATURE ESTIMATION

Consider a time-domain signal, $g(t)$, with $t \in [a, b]$, which can be mapped to a normalized time-domain signal, $y(x)$, such that $x \in [-1, +1]$.

$$y(x) \triangleq g\left(\frac{b-a}{2}x + \frac{a+b}{2}\right)$$

We can approximate the signal $y(x)$ using a finite weighted sum of polynomials, specifically, we use Chebyshev polynomials as presented in the work in [27], as,

$$y(x) \approx \tilde{y}(x) \triangleq \sum_{k=0}^{K-1} c_k T_k(x) \;\; \forall \; |x| \leq 1 \tag{1}$$

where the c_k are a set of K Chebyshev coefficients approximating the original signal and the $T_k(x)$ are the Chebyshev polynomials of the first kind defined as:

$$T_k(\cos(\theta)) = \cos(k\theta) \;\; \forall \;\; 0 \leq k < \infty$$

The discretized version of these polynomials form an orthogonal basis set [28]:

$$\sum_{n=0}^{N-1} T_i(x_n) T_j(x_n) = \begin{cases} 0 & i \neq j \\ \frac{1}{2-\delta_i} N & i = j \end{cases} \tag{2}$$

where δ_i is the Kronecker delta function of k, and:

$$x_n \triangleq \cos\left((n + \tfrac{1}{2})\frac{\pi}{N}\right) \qquad 0 \leq n < N \tag{3}$$

where $N \geq K$ is the number of time domain points used to compute the coefficients. Note that the orthogonality property does not hold at the more usual uniform samples in time but rather at these specific time points $\{x_n\}$. Accordingly, we can compute the coefficients as:

$$c_k = \frac{2-\delta_k}{N} \sum_{n=0}^{N-1} y_n T_k(x_n) \;\; \forall \;\; 0 \leq k < K \tag{4}$$

where $y_n \triangleq y(x_n)$ are the samples of y taken at the orthogonal time points x_n.

It is important to note the $\{x_n\}$ are more concentrated near the boundaries $x_n \simeq \pm 1$ compared to near the origin $x_n \simeq 0$. Fig. 2a shows the location of $\{x_n\}$ points on an ECG beat using (3). It can be seen that the distribution of these points is mostly concentrated towards the edges of the ECG beat, whereas the highest activity of the QRS complex lies around the R peak. The impact of this is that the approximation in (1) is poor if the c_k are computed using these x_n points directly. To address this issue, we introduce a pre-processing step that first applies a windowing function to the ECG beat, followed by a rotation (in time) around the R peak. The purpose of the windowing is to taper off the edges of the ECG beat before rotation to eliminate an unwanted discontinuity post-rotation. Although many windowing functions are possible, we chose to use the following raised cosine window function defined on the interval $x \in [-1, 1]$:

$$w(x) = \begin{cases} 1 & |x| < (1-\beta) \\ \frac{1}{2}\left(1 + \cos\left(\pi \frac{|x| - (1-\beta)}{\beta}\right)\right) & \text{elsewhere} \end{cases}$$

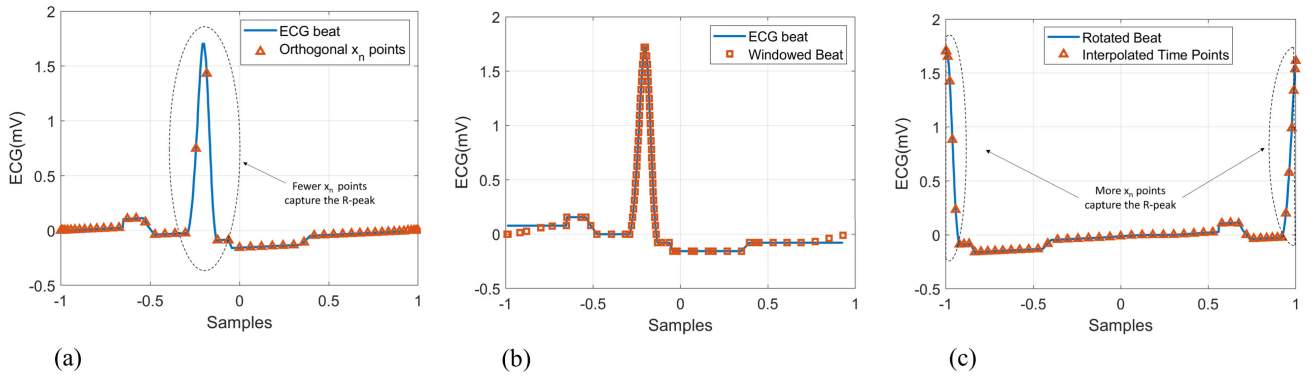

FIGURE 2. (a) An example of the x_n time points on an ECG beat for N=50, (b) effect of windowing, and (c) the rotated beat and new orthogonal points.

where β is the roll-off factor and signifies the percentage of the signal being tapered off. In this work, we set $\beta = 30\%$. Together, the windowing and rotation operation can be summarized in the following equation:

$$y(x) \leftarrow \begin{cases} y'(x-1+R) & x > -R \\ y'(x+1+R) & x \leq -R \end{cases}$$

where $y'(x) \triangleq w(x)y(x)$ is the windowed version of $y(x)$, and $R \in [-1, 1]$ is the position in time of the R-peak. Accordingly, the beat is now rotated (circularly shifted) around the R-peak such that the R-peak is now positioned near the boundaries at $x = \pm 1$; this corresponds to the highest density of orthogonal points x_n as per (3) meaning that the x_n time points will now be 'focused' on the R-peak.

This is illustrated in Fig. 2 where N=50 time points, x_n, are shown with and without these pre-processing steps. Firstly, in Fig. 2a, the position of the x_n with respect to the original ECG beat is shown - it can be seen that the R-peak is not well-captured, having only 2 samples. Fig. 2b shows the effect of windowing to taper off the edges. Finally, Fig. 2c shows that after rotation, there are now 11 samples in the region of the R peak, making any subsequent processing more accurate.

B. EFFICIENT COEFFICIENT CALCULATION WITH DISCRETE COSINE TRANSFORM

Computing the coefficients, denoted as $\{c_k\}$, using the direct method, as outlined in equation (4), exhibits a computational complexity of $O(NK)$ and necessitates prior knowledge of the values of $T_k(x_n)$ for $0 \leq k < K$ and $0 \leq n < N$. In contrast, we propose utilizing the Discrete Cosine Transform (DCT) [29], which offers a more efficient computation with a complexity of $O(N \log N)$. By employing equation (3) in equation (4), we obtain:

$$c_k = \frac{2-\delta_k}{N} \sum_{n=0}^{N-1} y_n \cos\left(k(n+\tfrac{1}{2})\frac{\pi}{N}\right)$$

This summation is just the length N DCT(Type II) of the vector $\vec{y}$ where $\{\vec{y}\}_n \triangleq y_n$

$$c_k = \frac{2-\delta_k}{N}\{DCT(\vec{y})\}_k \;\; \forall \;\; 0 \leq k < N \tag{5}$$

Here, $DCT(\vec{y})_k$ represents the k-th DCT coefficient of the vector $\vec{y}$. It is important to highlight that the computational complexity of our DCT method is independent of K. This is because we compute all N DCT coefficients and subsequently discard the last $N - K$ coefficients to obtain our desired set of K Chebyshev coefficients. An essential advantage of our DCT-based approach is the elimination of the need to pre-compute or store the $T_k(x_n)$ values, which would be particularly burdensome for resource-constrained IoT devices.

C. CLASS-ORIENTED CLASSIFIERS

In the context of ECG classification using functional approximation features, we propose employing three machine learning algorithms: a k-nearest neighbour classifier, a support vector machine, and an artificial neural network.

1) K-NEAREST NEIGHBORS

To design a k-NN classifier, we utilized the MATLAB Classification Learner toolbox, setting k equal to 3. The choice of k was determined through simulations across the range of $k = [1, 2, 3, \ldots, 30]$. As shown in Figure 3, the cross-validation and test errors were minimized when k was set to 3. Thus, we adopted a 3-NN classifier for our feature set classification. We also used a 70:30 training-to-test ratio and employed 10-fold cross-validation during training.

2) SUPPORT VECTOR MACHINES

For SVM classification, we utilized the LibSVM library within MATLAB to train a one-vs-one Gaussian SVM model. We employed a cross-validation grid search to optimize the Gaussian model parameters, resulting in a cost value of 3 and a gamma value of 1. A 70:30 split ratio between the training and test sets was also applied. This model involved a total of 12,898 trained support vectors.

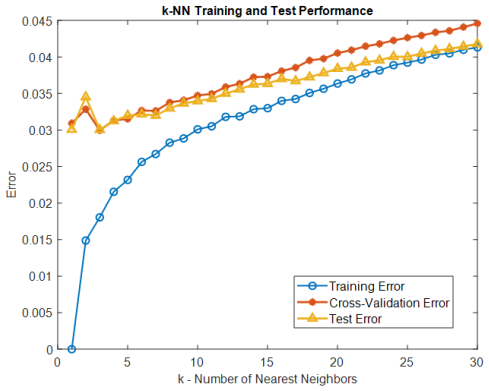

FIGURE 3. The training, cross-validation and test error as a function of k nearest neighbours for the k-NN classifier.

3) ARTIFICIAL NEURAL NETWORK

In this approach, we utilized the artificial neural network model described in [27]. The architecture consists of three hidden layers with 128, 64, and 32 neurons and an output layer with 4 neurons representing class labels. The number of hidden layers and the number of neurons were selected after several simulations, considering options ranging from one to five hidden layers and 8-256 neurons per layer.

We adopted a training-test split ratio of 70:30, allocating an additional 10% as a validation set from the training data. The model was trained using the Adam optimizer, sparse categorical cross-entropy loss, and a batch size of 64. Early stopping was implemented to prevent overfitting, and we employed synthetic minority oversampling [30] to address class imbalance.

III. EXPERIMENTAL SETUP

A. ORTHOGONAL TIME POINTS: CHOICE OF N

To determine the minimum number of time points required for computing the approximation coefficients and to showcase the significance of pre-processing steps (windowing and rotation), we conducted experiments with and without these pre-processing steps. In each case, we evaluated the root mean square (RMS) difference [17] between $y(x)$ and its approximation $\tilde{y}(x)$ as defined in (1). These experiments were carried out using the MIT-BIH Arrhythmia Database [31] for various values of N, and the results are presented in Fig. 4.

In Fig. 4a, the beats were interpolated to orthogonal time points without any pre-processing, and converted to Chebyshev coefficients. Next, the beat was reconstructed from the coefficients and the percentage RMS difference was calculated compared to the original beat. In Fig. 4b the same procedure was repeated, but this time, the windowing and rotation pre-processing steps were applied before interpolation. Comparing the mean PRD values (shown in blue) it can be seen in Fig. 4a, that the percentage RMS difference converges to 2.52% when using N=300 time points without

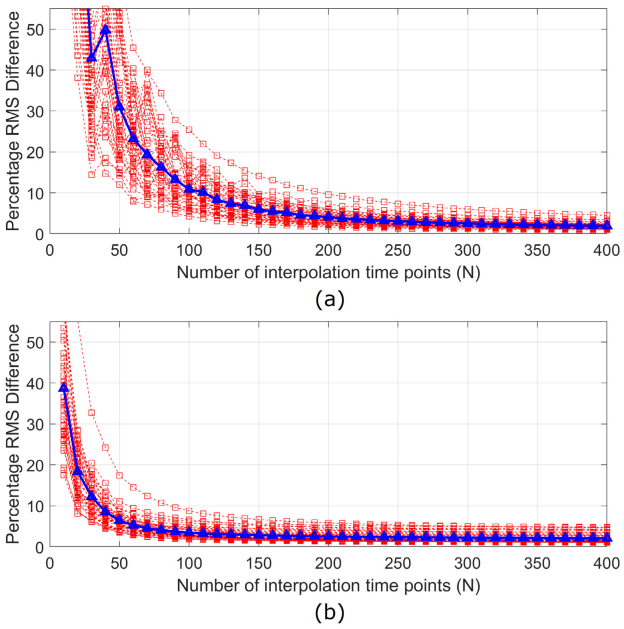

FIGURE 4. The percentage RMS difference as a function of N (number of interpolation points) when a) windowing and rotation are not used, and b) when windowing and rotation are used. (Note: The blue triangles represent the average over all records in the MIT-BIH dataset.).

the pre-processing steps. Whereas, with the pre-processing steps, in Fig. 4b, the percentage RMS difference converges faster to 2.56% at N=200 time points. Thus confirming the usefulness of these proposed pre-processing steps. For the rest of this article, a value of N=200 is used throughout.

B. BANDWIDTH ANALYSIS: CHOICE OF K

The approximation in (1), where we essentially zero the Chebyshev coefficients for $k > K$, is analogous to removing high-frequency terms in a Fourier series style expansion, i.e. it represents an implicit low-pass filtering operation. To quantify this concretely and to serve as an aid in selecting a suitable value of K we derive in this section, a closed-form expression of the frequency content captured by the Chebyshev polynomials. We show that, for any application, the choice of K can be made simply by knowing the cut-off frequency one wishes to obtain.

The signal $\tilde{y}(x)$ can be approximated using the first K terms as:

$$\tilde{y}(x) \approx \sum_{k=0}^{K-1} c_k T_k(x)$$

Then in the frequency domain,

$$\tilde{Y}(\omega) = \mathscr{F}(\tilde{y}) = \sum_{k=0}^{K-1} c_k \hat{T}_k(\omega)$$

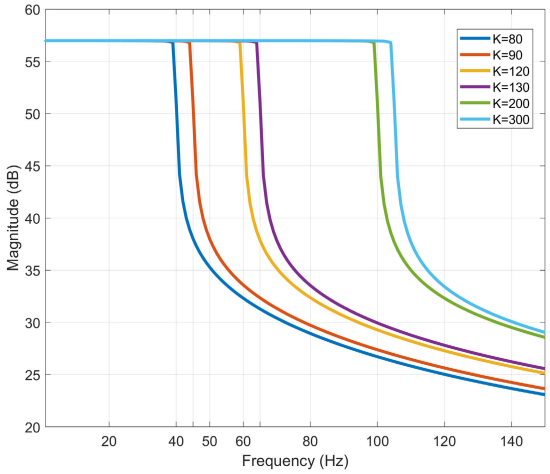

FIGURE 5. Spectrum for various choices of K used in the functional approximation.

where, $\hat{T}_k(\omega)$ is the Fourier transform of $T_k(x)$. Then, the energy spectral density of the signal is,

$$\begin{aligned} S_{\tilde{y}}(\omega) &= E\left[\left|\tilde{Y}(\omega)\right|^2\right] \\ &= E\left[\left|\sum_{k=0}^{K-1}\hat{T}_k(\omega)c_k\right|^2\right] \\ &= \sum_{i=0}^{K-1}\sum_{j=0}^{K-1}\left|\hat{T}_i(\omega)\hat{T}_j(\omega)\right|^2 E\left[\left|c_i c_j\right|^2\right] \end{aligned} \tag{6}$$

In general, the auto-correlation function $E[c_i c_j]$ is not known for arbitrary signals so the approach adopted here is to compute the spectrum of the output, i.e. $S_{\tilde{y}}(\omega)$ under the assumption that the input $\vec{y}$ is white. Accordingly, it is shown in Appendix A that:

$$E[c_i c_j] = \delta_{i-j}$$

Therefore, (6) can be reduced to:

$$S_{\tilde{y}}(\omega) = \sum_{k=0}^{K-1}\left|\hat{T}_k(\omega)\right|^2 \tag{7}$$

Fig. 5 illustrates this spectrum, $S_{\tilde{y}}(\omega)$, for various choices of K, the number of Chebyshev coefficients used in the functional approximation. It can be seen that the sum of K polynomials behaves like an implicit low-pass filter on the incoming signal. For example, for K=80 Chebyshev coefficients, the noise beyond 40 Hz is removed. Therefore, for the rest of this study, we choose K=80 as it captures the useful ECG bandwidth of 0.5-40Hz. Due to this implicit filtering effect, applications that employ this functional approximation technique may opt to remove filtering as a pre-processing step, as is the case for our work. Fig. 5 can be used as a guide for this purpose.

TABLE 2. Beat distribution in the combined MIT-BIH Arrhythmia and MIT-BIH Supraventricular Datasets.

Beat Type	Number of Beats	Percentage
N	90631	73.32%
S	14979	12.12%
V	17179	13.90%
F	826	0.67%

C. EVENT-DRIVEN DATASET

For the classification of ECG beats, the MIT-BIH Arrhythmia database [31] was used, which contains 48 two-channel recordings sampled at 360Hz with an 11-bit resolution. This dataset was non-uniformly sampled using a 7-bit LC-ADC with a 2385 Hz clock and a 6-bit clock timer as described in [27]. Using the recommendations by the Association for the Advancement of Medical Instrumentation (AAMI) [32], the beats were organized into four major classes, i.e. normal (N), supraventricular (S), ventricular (V), and fusion (F) beats. Furthermore, the four paced records 102, 104, 107 and 217 were excluded from the analysis.

There is an inherent class imbalance in this dataset where the majority class (N) is represented by 83% beats, and the smallest class (F) is represented by less than 1% beats. To overcome this class imbalance, we supplemented this data with the S, V and F types beats from the MIT-BIH Supraventricular Arrhythmia Database [33]. This database is sampled at 128Hz. Therefore, it was first resampled to 360Hz before non-uniform sampling using the 7-bit LC-ADC as described above. The new class distribution with combined beats from both datasets is shown in Table 2. Next, using N=200 time points and K=80 Chebyshev coefficients, each beat was converted to 81 approximation coefficients using (4). The feature set was normalized before training, validation and testing of classifiers.

D. EVALUATION METRICS

All classifiers were evaluated for Accuracy (ACC), sensitivity (SEN or recall), positive predictivity (PPV or precision), and false positive rate (FPR), which are defined as:

$$\begin{aligned} ACC &= \frac{(TP+TN)}{(TP+FP+FN+TN)} \\ SEN &= \frac{TP}{(TP+FN)} \\ PPV &= \frac{TP}{(TP+FP)} \\ FPR &= \frac{FP}{(FP+TN)} \end{aligned}$$

where FP, FN, TP, and TN are the number of false positives, false negatives, true positives, and true negatives per class.

In addition to ACC, SEN, PPV and FPR, the classifiers are also evaluated using the F1 scores. The F1 score provides a combined evaluation of SEN and PPV, representing their harmonic mean. It is a valuable metric for assessing both

TABLE 3. Classification results using the three machine-learning algorithms.

Model	Class	ACC(%)	SEN(%)	PPV(%)	FPR(%)	F1
k-NN	N	98.43	99.53	98.36	4.62	0.98
	S	97.60	88.42	91.59	1.12	0.89
	V	98.24	92.23	94.73	0.81	0.93
	F	99.72	70.09	82.41	0.10	0.75
SVM	N	98.47	99.18	98.75	5.4	0.98
	S	97.60	86.59	93.21	1.31	0.89
	V	98.03	95.19	90.80	0.28	0.92
	F	99.79	72.36	90.16	0.27	**0.80**
ANN	N	98.45	99.32	98.58	3.97	**0.98**
	S	97.69	89.47	91.35	1.17	**0.90**
	V	98.18	92.50	94.03	0.92	**0.93**
	F	99.72	72.22	81.25	0.11	0.76
ANN with SMOTE	N	98.04	98.47	98.87	3.14	0.98
	S	97.21	90.50	87.08	1.31	0.88
	V	98.07	92.13	93.59	0.28	0.92
	F	99.67	76.50	72.76	0.27	0.74

parameters simultaneously and is defined as:

$$F1 = 2 * \frac{(PPV * SEN)}{(PPV + SEN)}$$

In this analysis, two classification approaches are considered: class-oriented and patient-specific. The patient-specific approach demands a sufficient amount of labelled data from each new patient to train the classifier. This necessitates extended recordings and additional time for clinicians to assign and verify labels in long-term ECG recordings. Consequently, for this study, we opted for the class-oriented classification approach. In this approach, similar beats from all subjects are grouped for training and testing. One drawback of this approach is the variability observed in the same type of ECG beats from subject to subject, adding complexity to the classification task.

IV. RESULTS AND DISCUSSION

Table 3 shows the classification results using the three classifiers summarized in II-C. For the KNN, with a cross-validation loss of 0.031, F1 scores of 0.98, 0.89, 0.93 and 0.75 are achieved for the N, S, V and F classes, respectively. The k-NN was also tested using SMOTE to balance the dataset. However, no improvement in testing accuracies was observed. The SVM model achieved similar results for the N, S, and V classes but classified the smallest class F better with an F1-score of 0.80. Additionally, we tested the SVM model with SMOTE to balance the class distribution, which did not improve the results. Linear SVM models were also tested for classification performance. However, they failed to perform well in the smaller classes.

Table 3 also shows the ANN performance without SMOTE and with SMOTE to balance the class distribution.

Although the three classifiers gave very similar performances, the ANN combined with SMOTE had the highest sensitivities and lowest false-positive rates for the four classes. Furthermore, the SVM model had a similar performance to the k-NN model. Sensitivity, also known as recall, is considered the most important evaluation parameter in this classification problem as it represents the classifier's ability to correctly diagnose arrhythmias. For example, a high sensitivity in the S class represents correctly identified S-type beats in the record when it truly contained S-type beats.

TABLE 4. Gaussian SVM performance on the three majority classes.

Model	Class	ACC(%)	SEN(%)	PPV(%)	FPR(%)	F1
SVM	N	98.56	99.21	98.85	3.30	0.99
	S	97.61	86.59	93.38	0.86	0.89
	V	98.09	95.31	91.19	1.47	0.93
ANN	N	98.62	99.27	98.86	3.24	0.99
	S	97.60	89.27	90.97	1.23	0.90
	V	98.22	93.21	93.78	0.98	0.93

In terms of complexity, the k-NN model has a complexity of $O(nd)$, where n=85980 training data points and d=81 is the number of features in the training set. Therefore, the kNN requires close to 7 million parameters to be stored in memory for real-time classification. Next, the SVM model requires 12898×3 support vector coefficients and a 12898×81 matrix to store the 12898 support vectors. Overall, the SVM model requires a little over 100,000 parameters to be stored in memory for classification. Finally, the ANN model requires only 20,964 parameters for real-time classification.

While, practically, the ANN model appears to be the optimal choice for real-time on-device classification, all three models underscore the efficiency of the functional approximation feature set in representing event-driven ECG data. The highlighted F1-scores in Table 3 indicate the best-performing models for each class.

It's important to note that the relatively poorer performance of the F-class can be attributed to its representation in less than 1% of the overall dataset. For very imbalanced classes, most classifiers and class-balance techniques struggle to perform effectively, as observed in the limited improvement provided by SMOTE for the F-class. This class imbalance's impact is evident in the three-class results presented in Table 4 when using the Gaussian SVM. For this analysis, F-class beats were excluded from all records. These results show a slight improvement over those in Table 3 using Gaussian SVM and ANN but remain otherwise unaffected.

A. COMPARISON WITH PREVIOUS WORKS

Table 5 provides a performance comparison between this study and previous hardware-efficient designs. Two of these designs utilized uniformly sampled ECG data, while the others employed event-driven ECG. In this study, the ANN and Gaussian SVM models exhibited similar F1 scores for all four classes. However, the ANN model required approximately 79% fewer hardware resources than the Gaussian SVM model. Both models outperformed the ANN model in [27] and the 1D-CNN model in [17], both of which used a 7-bit level-crossing ADC with a 2385 Hz clock. The 1D-CNN [17] required 132,676 parameters and achieved a relatively lower F1 score (0.83) for S-type beats but slightly better F1 scores for F-type and V-type beats (0.84 and 0.96, respectively) compared to the Gaussian SVM and ANN models in this study. The ANN model in [27] required 20,964

TABLE 5. Comparison with previous works.

Study	Sampling	Model	Approach	#Params	Class	ACC(%)	SEN(%)	PPV(%)	FPR(%)	F1
This work	event-driven	ANN	class-oriented	20,964	N	98.45	99.32	98.58	3.97	**0.99**
					S	97.69	89.47	91.35	1.17	**0.90**
					V	98.18	92.50	94.03	0.92	**0.93**
					F	99.72	72.22	81.25	0.11	**0.76**
This work	event-driven	Gaussian SVM	class-oriented	100,000	N	98.47	99.18	98.75	5.4	0.98
					S	97.60	86.59	93.21	1.31	0.89
					V	98.03	95.19	90.80	0.28	0.92
					F	99.79	72.36	90.16	0.27	0.80
2022 Saeed et al. [27]	event-driven	ANN	class-oriented	20,964	N	97.83	98.22	99.34	5.40	0.99
					S	98.38	87.91	65.50	1.31	0.75
					V	99.39	95.15	96.33	0.28	0.96
					F	99.61	84.73	71.97	0.27	0.78
2021 Saeed et al. [17]	event-driven	1D-CNN	class-oriented	132,676	N	98.57	99.55	98.86	9.71	0.99
					S	99.13	76.98	90.01	0.37	0.83
					V	99.49	95.19	97.45	0.19	0.96
					F	99.74	80.48	87.56	0.10	0.84
2019 Zhao et al. [34]	event-driven	ANN	patient-specific	3,717	N	99.32	99.45	99.76	1.43	0.99
					S	99.70	97.75	94.39	0.23	0.96
					V	99.68	98.67	98.07	0.21	0.98
					F	98.87	49.03	87.80	0.14	0.63
2022 Janveja et al. [35]	uniform	ANN	patient-specific	8,415	S	88.60	86.45	-	17.79	-
					V	92.05	83.37	-	5.94	-
2019 Tang et al. [3]	uniform	Linear SVM	class-oriented	32	S	98.90	88.30	79.7	0.4	0.83
					V	99.00	91.1	81.3	0.6	0.92

Note: Highlighted F1 Scores (in bold) show the model with the best performance-complexity trade-off.

parameters and achieved lower F1 scores for S-type and F-type beats (0.75 and 0.78, respectively).

In [34], the ANN model used an 11-bit ADC and was analyzed using a patient-specific approach, requiring only 3,717 parameters to be stored in memory. This model achieved slightly better F1 scores for S-type and V-type beats at 0.96 and 0.98, respectively. However, the F1 score for F-type beats was the lowest among all models at 0.63, primarily due to the low sensitivity performance of F-type beats at 40.03%. The models in [3] and [35] utilized uniformly sampled ECG and reported results for S-type and V-type beats only. Unfortunately, the PPV parameter was not reported in [35], preventing direct comparison of F1 scores. The ANN model in this work required only 8,415 parameters and was evaluated using a patient-specific model. The class-wise performance of the class-oriented model was not reported in [35]. The classifier in [3] presented a very low-complexity linear SVM that required only 32 parameters. The best model, SkP-32, achieved F1 scores of 0.83 for S-type beats and 0.92 for V-type beats, with poorer PPV values compared to other works. Overall, the three-layered ANN model presented in Section II-C3 demonstrated the most balanced performance across all classes and required only 20,964 parameters for real-time classification. With more data available for the F-class, further improvements in results can be expected.

B. COMPLEXITY CONSIDERATION OF THE SYSTEM

To estimate the complexity inferred, we consider the event-driven classification system shown in Fig. 6. Analog ECG signal is sampled by the 7-bit level-crossing ADC, using the two thresholds, U_{QL} and L_{QL}. The two digital-to-analogue converters adapt the thresholds as the input ECG signal changes. We use a 2385Hz clock cycle and a 6-bit timer as described in [36]. The non-uniformly sampled ECG_{out} and the vector representing the time between consecutive samples, TI, are fed into an R-peak detector and a beat extractor. A low-complexity level-crossing-based QRS detector [10], [37] can be used here. The beat-extractor identifies all samples within a window of -260ms to +400ms about the R-peak. Note that the number of samples contained within this window is variable due to the event-driven nature of the LC-ADC. These samples are then fed into a linear interpolator that generates samples at the 200 orthogonal time points defined in (3). Approximately 400 multiplications (or equivalently divisions) operations are required to convert the 2D variable length vector [ECG_{out}, TI] to these orthogonal time points. As described in Section II-A, the windowing function requires 200 multiplications, and the rotation in time can be implemented for free by careful pre-rotation of the stored Chebyshev basis functions. Alternatively, the rotation step can also be absorbed into the stored Chebyshev polynomials (basis functions). Next, the 81 feature vector is computed by a dot product that requires using 200 multiplications per feature. In total, the feature extraction requires 400+200+81*200 $\approx$ 17k multiplications per ECG beat. Whereas, the pre-trained ANN-based classifier itself requires 21k multiplications (i.e. the number of parameters in the ANN). This final block in Fig. 6 produces a label per ECG beat, classifying them as normal (N) or abnormal (S, V or F). These complexity estimates are per-ECG beat, which for a typical subject of c.60 to 100 beats per minute would result in a complexity of approximately 0.1 MIPS.

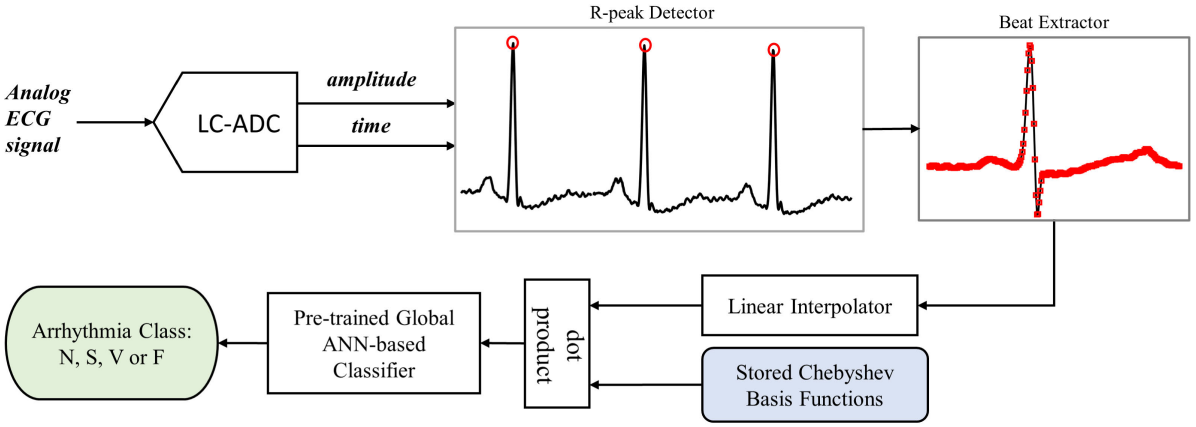

FIGURE 6. The event-driven electrocardiogram classification system with a level-crossing ADC, approximation coefficient features and a neural network classifier.

V. ECG SIGNAL RECONSTRUCTION

In an automated event-driven arrhythmia classification system, the arrhythmias detected by the system may necessitate further analysis by a specialist or practitioner to assess the underlying issues. Therefore, in this section, we propose and compare various methodologies for reconstructing a signal $\tilde{y}(x)$ at a set of N time points using a set of K Chebyshev coefficients. As presented in Section II-A, to compute the c_k coefficients using (4), the signal $y(x_n)$ must be taken at the orthogonal time points x_n represented by (3). Signals are not inherently sampled at these orthogonal time points. Therefore, interpolation techniques such as linear or cubic-spline interpolation must be used before computing the K Chebyshev coefficients. Table 6 summarizes the reconstruction methods presented below.

A. INVERSE DISCRETE COSINE TRANSFORM AND INTERPOLATION

By using (3) in (1), the signal $\tilde{y}(x)$ can be computed as,

$$\tilde{y}(x_n) = \sum_{k=0}^{K-1} c_k T_k(\cos\left((n+\tfrac{1}{2})\frac{\pi}{N}\right)) = \sum_{k=0}^{K-1} c_k \cos\left(k(n+\tfrac{1}{2})\frac{\pi}{N}\right)$$

This is equivalent to the inverse discrete cosine transform (iDCT) if we also include a scaling factor, such that,

$$\Rightarrow \tilde{\boldsymbol{y}} = \sqrt{\frac{N}{2}}\text{iDCT}\left(\boldsymbol{c'}\right)$$

where

$$\{\tilde{\boldsymbol{y}}\}_n \triangleq \tilde{y}(x_n) \quad \text{and} \quad \{\boldsymbol{c'}\}_k = \begin{cases} \sqrt{2}c_0 & k = 0 \\ c_k & 1 \le k < K \\ 0 & K \le k < N \end{cases}$$

The iDCT reconstruction method reconstructs the signal at orthogonal time points. Therefore, reconstruction using iDCT still requires interpolation to get to the desired time points.

B. ITERATIVE APPROACH

We can iteratively construct a vector b of length $K \times 1$ at any time point x, such that reconstruction of the signal is only dependant on its first two terms, as defined by the following algorithm:

Algorithm 1 Procedure for Computing $\tilde{y}(x)$ Given $\boldsymbol{c}$

Let $b_K = b_{K+1} = 0$
for $r = K-1 \rightarrow 0$ **do**
$b_r = c_r + 2xb_{r+1} - b_{r+2}$
end for
$\tilde{y}(x) = b_0 - x * b_1$

where, $\vec{c}$ is the vector of K coefficients. A more detailed analysis of this algorithm is presented in a previous study [36].

C. COMPARISON OF RECONSTRUCTION TECHNIQUES

Table 6 summarizes the three reconstruction methods presented above. We tested the three reconstruction techniques on record 234 of the MIT-BIH Arrhythmia dataset. The direct method with interpolation has a complexity of O (NK) and an average reconstruction error of 4.821% overall beats. If interpolation is to be avoided, this method requires prior knowledge of the Chebyshev polynomials at targeted time points or the capability to compute the polynomials at runtime. The iDCT approach has the computational complexity of O ($N \log K$) and is restricted to the N orthogonal time points and requires interpolation to get to the desired time points. However, it is much faster than the direct method. Finally, the iterative approach has a complexity of O ($N \log N$) and can be computed at any arbitrary set of N time points on the continuous range $[-1, +1]$. Furthermore, the iterative approach had a reconstruction error of only 0.008%.

TABLE 6. Comparison of signal reconstruction techniques.

Method	RMS Difference	Complexity	Comment
Direct & interpolation	4.821%	O (NK)	To avoid interpolation, the Chebyshev polynomials need to be known at the required time points in advance or we need the capability of computing them at run-time (expensive).
iDCT & interpolation	4.827%	O $(N \log K)$	The iDCT yields $\tilde{y}(x_n)$. These then need to be interpolated to get the desired time points.
Iterative	0.008%	O $(N \log N)$	Works quickly and accurately for any set of N points.

VI. CONCLUSION

This work presented an efficient way to reduce high-dimensional data streams into a compact set of features that can be classified using low-complexity machine learning classifiers. Functional approximation and Chebyshev polynomials were used to estimate a small feature set to classify the ECG beats in real-time, which can be applied to uniformly or non-uniformly sampled signals. A closed-form expression was derived that represents the frequency content captured by the Chebyshev polynomials. We have shown that Chebyshev polynomials implicitly apply low-pass filtering to signals. Using 80 Chebyshev coefficients, the 3 dB cut-off frequency of 40 Hz for ECG signals was achieved. It also demonstrated the use of discrete cosine transforms for faster calculations of Chebyshev coefficients. In addition, three machine learning algorithms for classifying ECG beats into four classes (N, S, V, and F) using the 81 Chebyshev coefficients were presented.

The ANN performed best for all classes and required the fewest number of training parameters (20,964), making it the most practical choice for real-time classification. Compared to previous works, the ANN model presented here, which uses a class-oriented classification approach, performed the best among all uniformly and event-driven classifiers developed for real-time ECG classification. This model had an overall F1-score of 0.99, 0.90, 0.93, and 0.76 for N, S, V, and F classes. The results for the smallest class (F) in our model, representing 0.67% of all beats in the dataset, could be further improved if additional beats were available for the class. Finally, an iterative algorithm for fast and accurate reconstruction of ECG beats at any point in time and at any resolution was presented, which may be useful for further analysis of ECG data by physicians.

APPENDIX A
COMPUTATION OF COEFFICIENT CROSS-CORRELATION FUNCTION

For the evaluation of (6), we know that $c_i c_j = 0 \ \ \forall\, i, j \geq k$ and $c_k = \vec{d}_k \cdot \vec{y}$. Here, $\vec{d}_k$ is the k^{th} row of the DCT matrix in (5) and we assume, that $\vec{y}$ is a column vector containing a white signal. Then,

$$\begin{aligned} c_i c_j &= (\vec{d}_i \cdot \vec{y})(\vec{d}_j \cdot \vec{y}) \\ &= (\sum_l d_{i,l} y_l)(\sum_r d_{j,r} y_r) \\ &= \sum_l d_{i,l} d_{j,l} y_l^2 + \sum_l \sum_{r \neq l} d_{i,l} d_{j,r} y_l y_r \end{aligned}$$

Under the assumption that the input signal $\vec{y}$ is white then we can say $E[|\vec{y}|^2] = \mathbf{I}$, i.e.:

$$E[y_l y_r] = \delta_{l-r}$$

where δ_k is the Kronecker delta function. Thus, the expected value of the $c_i c_j$ becomes:

$$\begin{aligned} E[c_i c_j] &= \sum_l d_{i,l} d_{j,l} \\ &= \vec{d}_i \cdot \vec{d}_j \\ &= \delta_{i-j} \end{aligned}$$

REFERENCES

[1] G. Lippi, F. Sanchis-Gomar, and G. Cervellin, "Global epidemiology of atrial fibrillation: An increasing epidemic and public health challenge," *Int. J. Stroke*, vol. 16, no. 2, pp. 217–221, Feb. 2021.

[2] J. Malik, O. C. Devecioglu, S. Kiranyaz, T. Ince, and M. Gabbouj, "Real-time patient-specific ECG classification by 1D self-operational neural networks," *IEEE Trans. Biomed. Eng.*, vol. 69, no. 5, pp. 1788–1801, May 2022.

[3] X. Tang, Z. Ma, Q. Hu, and W. Tang, "A real-time arrhythmia heartbeats classification algorithm using parallel delta modulations and rotated linear-kernel support vector machines," *IEEE Trans. Biomed. Eng.*, vol. 67, no. 4, pp. 978–986, Apr. 2020.

[4] S. Kiranyaz, T. Ince, and M. Gabbouj, "Real-time patient-specific ECG classification by 1-D convolutional neural networks," *IEEE Trans. Biomed. Eng.*, vol. 63, no. 3, pp. 664–675, Mar. 2016.

[5] S. M. Abubakar, W. Saadeh, and M. A. B. Altaf, "A wearable long-term single-lead ECG processor for early detection of cardiac arrhythmia," in *Proc. Design, Autom. Test Eur. Conf. Exhib. (DATE)*, Mar. 2018, pp. 961–966.

[6] J. Duforest, B. Larras, D. John, O. Martens, and A. Frappé, "Slope-based event-driven feature extraction for cardiac arrhythmia classification," in *Proc. IEEE Biomed. Circuits Syst. Conf. (BioCAS)*, Oct. 2021, pp. 1–4.

[7] X. Tang and W. Tang, "An ECG delineation and arrhythmia classification system using slope variation measurement by ternary second-order delta modulators for wearable ECG sensors," *IEEE Trans. Biomed. Circuits Syst.*, vol. 15, no. 5, pp. 1053–1065, Oct. 2021.

[8] Y. Li, A. L. Mansano, Y. Yuan, D. Zhao, and W. A. Serdijn, "An ECG recording front-end with continuous-time level-crossing sampling," *IEEE Trans. Biomed. Circuits Syst.*, vol. 8, no. 5, pp. 626–635, Oct. 2014.

[9] T. Marisa, T. Niederhauser, A. Haeberlin, R. A. Wildhaber, R. Vogel, J. Goette, and M. Jacomet, "Pseudo asynchronous level crossing ADC for ECG signal acquisition," *IEEE Trans. Biomed. Circuits Syst.*, vol. 11, no. 2, pp. 267–278, Apr. 2017.

[10] N. Ravanshad, H. Rezaee-Dehsorkh, R. Lotfi, and Y. Lian, "A level-crossing based QRS-detection algorithm for wearable ECG sensors," *IEEE J. Biomed. Health Informat.*, vol. 18, no. 1, pp. 183–192, Jan. 2014.

[11] M. Tlili, M. Ben-Romdhane, A. Maalej, F. Rivet, D. Dallet, and C. Rebai, "Level-crossing ADC design and evaluation methodology for normal and pathological electrocardiogram signals measurement," *Measurement*, vol. 124, pp. 413–425, Aug. 2018.
[12] J. Van Assche and G. Gielen, "A 10.4-enob 0.92–5.38 μw event-driven level-crossing ADC with adaptive clocking for time-sparse edge applications," in *Proc. IEEE 48th Eur. Solid State Circuits Conf. (ESSCIRC)*, Sep. 2022, pp. 261–264.
[13] R. Wei, F. Lin, and Q. Chen, "A continuous time level-crossing ADC with adaptive sampling for biomedical application," *IEICE Electron. Exp.*, vol. 19, no. 7, 2022, Art. no. 20220072.
[14] X. Tang, M. Renteria-Pinon, and W. Tang, "Second-order level-crossing sampling analog to digital converter for electrocardiogram delineation and premature ventricular contraction detection," *IEEE Trans. Biomed. Circuits Syst.*, vol. 17, no. 6, pp. 1342–1354, Dec. 2023.
[15] S. Lin, C. Lin, and Q. Chen, "A low-power level-crossing ADC for biosignal acquisition," *J. Phys., Conf.*, vol. 2524, no. 1, Jun. 2023, Art. no. 012022.
[16] X. Tong, Y. Wei, W. Mao, and X. Xin, "A 200 Hz-to-10 kHz bandwidth 11.83-ENOB level-crossing ADC with single continuous-time comparator," *Microelectron. J.*, vol. 126, Aug. 2022, Art. no. 105482.
[17] M. Saeed, Q. Wang, O. Martens, B. Larras, A. Frappe, B. Cardiff, and D. John, "Evaluation of level-crossing ADCs for event-driven ECG classification," *IEEE Trans. Biomed. Circuits Syst.*, vol. 15, no. 6, pp. 1129–1139, Dec. 2021.
[18] M. Tlili, A. Maalej, M. Ben-Romdhane, M. C. Bali, F. Rivet, D. Dallet, and C. Rebai, "Level-crossing ADC modeling for wireless electrocardiogram signal acquisition system," in *Proc. IEEE Int. Instrum. Meas. Technol. Conf.*, May 2016, pp. 1–5.
[19] A. M. Price-Whelan, M. A. Agüeros, A. P. Fournier, R. Street, E. O. Ofek, K. R. Covey, D. Levitan, R. R. Laher, B. Sesar, and J. Surace, "Statistical searches for microlensing events in large, non-uniformly sampled time-domain surveys: A test using palomar transient factory data," *Astrophysical J.*, vol. 781, no. 1, p. 35, Jan. 2014.
[20] A. Aldroubi and K. Gröchenig, "Nonuniform sampling and reconstruction in shift-invariant spaces," *SIAM Rev.*, vol. 43, no. 4, pp. 585–620, Jan. 2001.
[21] G. Hennenfent and F. J. Herrmann, "Seismic denoising with nonuniformly sampled curvelets," *Comput. Sci. Eng.*, vol. 8, no. 3, pp. 16–25, May 2006.
[22] P. Babu and P. Stoica, "Spectral analysis of nonuniformly sampled data—A review," *Digit. Signal Process.*, vol. 20, no. 2, pp. 359–378, Mar. 2010.
[23] G. Plonka, D. Potts, G. Steidl, and M. Tasche, "Fast Fourier transforms for nonequispaced data," in *Numerical Fourier Analysis*. Cham, Switzerland: Springer, 2018, pp. 377–419.
[24] L. Greengard and J.-Y. Lee, "Accelerating the nonuniform fast Fourier transform," *SIAM Rev.*, vol. 46, no. 3, pp. 443–454, Jan. 2004.
[25] J. A. Fessler and B. P. Sutton, "Nonuniform fast Fourier transforms using min-max interpolation," *IEEE Trans. Signal Process.*, vol. 51, no. 2, pp. 560–574, Feb. 2003.
[26] F. Melchert, U. Seiffert, M. Biehl, B. Hammer, T. Martinetz, and T. Villmann, "Functional approximation for the classification of smooth time series," in *Proc. GCPR Workshop New Challenges Neural Comput.*, 2016, p. 4.
[27] M. Saeed, O. Märtens, B. Larras, A. Frappé, D. John, and B. Cardiff, "Event-driven ECG classification using functional approximation and Chebyshev polynomials," in *Proc. IEEE Biomed. Circuits Syst. Conf. (BioCAS)*, Oct. 2022, pp. 595–599.
[28] J. C. Mason and D. C. Handscomb, *Chebyshev Polynomials*. Boca Raton, FL, USA: CRC Press, 2002.
[29] N. Ahmed, T. Natarajan, and K. R. Rao, "Discrete cosine transform," *IEEE Trans. Comput.*, vol. COM-100, no. 1, pp. 90–93, Jan. 1974.
[30] N. V. Chawla, K. W. Bowyer, L. O. Hall, and W. P. Kegelmeyer, "SMOTE: Synthetic minority over-sampling technique," *J. Artif. Intell. Res.*, vol. 16, pp. 321–357, 2002.
[31] A. L. Goldberger, L. A. N. Amaral, L. Glass, J. M. Hausdorff, P. C. Ivanov, R. G. Mark, J. E. Mietus, G. B. Moody, C.-K. Peng, and H. E. Stanley, "PhysioBank, PhysioToolkit, and PhysioNet: Components of a new research resource for complex physiologic signals," *Circulation*, vol. 101, no. 23, pp. 215–220, Jun. 2000.
[32] EC57, *Testing and Reporting Performance Results of Cardiac Rhythm and ST Segment Measurement Algorithms*, Assoc. Advancement Med. Instrum., Arlington, VA, USA, 1998.
[33] S. D. Greenwald, R. S. Patil, and R. G. Mark, *Improved Detection and Classification of Arrhythmias in Noise-Corrupted Electrocardiograms Using Contextual Information*, 1990, pp. 461–464.
[34] Y. Zhao, Z. Shang, and Y. Lian, "A 13.34 μW event-driven patient-specific ANN cardiac arrhythmia classifier for wearable ECG sensors," *IEEE Trans. Biomed. Circuits Syst.*, vol. 14, no. 2, pp. 186–197, Apr. 2020.
[35] M. Janveja, R. Parmar, M. Tantuway, and G. Trivedi, "A DNN-based low power ECG co-processor architecture to classify cardiac arrhythmia for wearable devices," *IEEE Trans. Circuits Syst. II, Exp. Briefs*, vol. 69, no. 4, pp. 2281–2285, Apr. 2022.
[36] M. Saeed, D. John, and B. Cardiff, "Accurate reconstruction of ECG signals using Chebyshev polynomials," in *Proc. 29th IEEE Int. Conf. Electron., Circuits Syst. (ICECS)*, Oct. 2022, pp. 1–2.
[37] S. A. H. Sabzevari, N. Ravanshad, and H. Rezaee-Dehsorkh, "An ultra-low-power QRS-detection system based on level-crossing sampling," in *Proc. Electr. Eng. (ICEE), Iranian Conf.*, May 2018, pp. 1456–1461.

MARYAM SAEED (Member, IEEE) received the B.S. degree in telecommunication engineering from the National University of Computer and Emerging Sciences, Lahore, and the M.S. degree in electrical engineering from the National University of Sciences and Technology, Islamabad. She is currently a Ph.D. Scholar with the University College Dublin and a Schlumberger Faculty for the Future Fellow. Her current research interests include designing arrhythmia classifiers for low power circuits using event-driven ADCs, signal processing, and machine learning. Previously, she has worked on neural spike sorting for implanted brain circuits and EEG data acquisition for biomedical applications.

OLEV MÄRTENS (Senior Member, IEEE) was born in Tallinn, Estonia, in 1960. He received the Diploma in Engineering degree (cum laude) in electronics and the Ph.D. degree from the Tallinn University of Technology (TalTech), in 1983 and 2000, respectively. He has experience in the industrial research and development, and since 2000, in academy, being a Senior and Lead Researcher and he is currently an Associate Professor in measurement electronics with the Thomas Johann Seebeck Department of Electronics, TalTech.

BENOIT LARRAS (Member, IEEE) was born in Nancy, France, in 1988. He received the Engineering degree, the master's degree in telecommunications, and the Ph.D. degree in electrical engineering from IMT Atlantique, Brest, France, in 2012 and 2015, respectively. He is currently an Associate Professor with the Electronics Team, Junia, Lille, France. His research interests include analog/mixed-signal IC design and the circuit implementation of neural networks and associative memories, in the context of "near-sensor computing" and "edge computing." He is a co-recipient of a Best Paper at the IEEE AICAS2020 Conference.

ANTOINE FRAPPÉ (Senior Member, IEEE) received the Graduate degree from Institut SupÉrieur d'Electronique du Nord (ISEN), Lille, France, in 2004, and the M.Sc., Ph.D., and H.D.R. (French highest academic) degrees in electrical engineering from the University of Lille, France, in 2004, 2007, and 2019, respectively. Since 2004, he has been a member of the Silicon Microelectronics Group, Institute of Electronics, Microelectronics, and Nanotechnologies (IEMN), Villeneuve d'Ascq, France. He obtained a Fulbright Grant, in 2008, to pursue research in communication systems with the Berkeley Wireless Research Center (BWRC), UC Berkeley, CA, USA. He is currently an Associate Professor with Junia ISEN, Lille, France, leading the Electronics Team. His research interests include digital RF transmitters, high-speed converters, mixed-signal design for RF and mmW communication systems, energy-efficient integrated systems, event-driven, and neuro-inspired circuits for embedded machine learning. He was a co-recipient of the Best Student Paper Award at the 2011 Symposium on VLSI Circuits, the Best Paper Award at the 2020 IEEE AICAS Conference, and the Industrial Best Paper Award at the 2021 IEEE RFIC Symposium. He plays an active role as a Board Member of the France Section of the IEEE Circuits and Systems Society and a Counselor of the IEEE Lille Student Branch.

DEEPU JOHN (Senior Member, IEEE) received the B.Tech. degree in electronics and communication engineering from the University of Kerala, India, in 2002, and the M.Sc. and Ph.D. degrees in electrical engineering from the National University of Singapore, Singapore, in 2008 and 2014, respectively. He is currently an Assistant Professor with the School of Electrical and Electronics Engineering, University College Dublin, Ireland. He was a Postdoctoral Researcher with the Bioelectronics Laboratory, National University of Singapore, from 2014 to 2017. Previously, he was a Senior Engineer with Sanyo Semiconductors, Gifu, Japan. He is a recipient of the Institution of Engineers Singapore Prestigious Engineering Achievement Award, in 2011, the Best Design Award at the Asian Solid-State Circuit Conference, in 2013, and the IEEE Young Professionals, Region 10 Individual Award, in 2013. He served as a member of the Organizing Committee/Technical Program Committee for several IEEE conferences, including TENCON, ASICON, ISCAS, BioCAS, and ICTA. He is a reviewer of several IEEE journals and conferences. He served as a Guest Editor for IEEE TRANSACTIONS ON CIRCUITS AND SYSTEMS I: REGULAR PAPERS and IEEE OPEN JOURNAL OF CIRCUITS AND SYSTEMS. He serves as an Associate Editor for IEEE TRANSACTIONS ON BIOMEDICAL CIRCUITS AND SYSTEMS and *International Journal of Circuit Theory and Applications* (Wiley). His research interests include low-power biomedical circuit design, energy-efficient signal processing, and edge computing.

BARRY CARDIFF (Senior Member, IEEE) received the B.Eng., M.Eng.Sc., and Ph.D. degrees in electronic engineering from University College Dublin, Ireland, in 1992, 1995, and 2011, respectively. He was a Senior Design Engineer/Systems Architect with Nokia, from 1993 to 2001, moving to Silicon & Software Systems (S3 group) thereafter as a Systems Architect in their research and development division focused on wireless communications and digitally assisted circuit design. Since 2013, he has been an Assistant Professor with University College Dublin. His research interests include digitally assisted circuit design and signal processing for wireless and optical communication systems. He holds several U.S. patents related to wireless communication.